THE ASTROPHYSICAL JOURNAL, 430:581–594, 1994 August 1

A SUMMARY OF EXTREME SCATTERING EVENTS AND A DESCRIPTIVE MODEL

R. FIEDLER,[1] B. DENNISON,[2] K. J. JOHNSTON,[1] E. B. WALTMAN,[1] AND R. S. SIMON[1,3]

Received 1991 January 7; accepted 1994 January 28

ABSTRACT

An ongoing monitoring program of compact extragalactic radio sources over the past 11 years has revealed many instances of unusual variations that cannot be explained using the standard models for intrinsic variability or normal refractive interstellar scintillation. The observations included simultaneous daily measurements at 2.695 and 8.085 GHz of 40 to 150 sources using the Green Bank interferometer over the period 1979–1989. Approximately 330 sources were also monitored with the NRAO 300 foot radio telescope at 3.25 and 4.675 GHz over the 6 month period 1987 December to 1988 May. In total, 594 source-years of observations have been obtained, of which 4.8 yr constitutes the total time span of unusual variability. The unusual variations, denoted as extreme scattering events (ESEs), are summarized here. The most striking property of ESEs is their frequency dependence, in which departures from the quiescent flux density (by as much as 50% at 2.7 GHz) have no counterpart at 8.1 GHz. The single exception occurred in the 8.1 GHz light curve of 0954+658, which showed spiky variations during the 2.7 GHz event. To date, 10 ESEs have been tentatively identified in the 2.7 GHz light curves of nine quasars. These ESEs appear to occur preferentially near loops in the Galactic foreground brightness distribution. A simple model based on diffraction or refraction through Galactic regions of unusually high electron density turbulence is presented.

Subject headings: ISM: structure — radio continuum: galaxies — turbulence

1. INTRODUCTION

Extreme scattering events (ESEs) are a new class of variations at gigahertz frequencies, possibly caused by strong ray path distortions in the interstellar medium (ISM). The first reported ESEs (Fiedler et al. 1987a) occurred in the light curves of the quasars 0954+658, 1502+106, and 1611+343. At 2.7 GHz, these events are qualitatively similar in shape, each having a flat-bottomed minimum with surrounding maxima (see Fig. 1). Only one of these events (in 0954+658) was apparent at the higher frequency observed (8.1 GHz), where the light curve shows four very strong spikes during the flat-bottomed minimum at 2.7 GHz. We have tentatively identified ESEs in the light curves of six more quasars and found that there is a greater variety in event shape than was at first apparent. An inspection of the events illustrated in Figure 1 shows a broad range in shapes, including brief maxima bracketing an extended flat-bottomed minimum, a rounded minimum with, or without, bracketing maxima, and variations that appear as a grouping of two or more events.

We have dubbed the unusual variations "extreme scattering events," reflecting a statistical approach in modeling these events, in which ray path distortions are produced by a large number of electron density fluctuations confined to a localized region of the ISM. However, Romani, Blandford, & Cordes (1987) have pointed out a different approach which relies on a localized structure in the ISM with a smooth, Gaussian profile of excess electron density. Whether an ensemble of density enhancements, or a single smoothly varying density profile, is responsible for the observed variations remains to be resolved. In this paper, we will refer to an unusual variation as an ESE and to the related ISM structure as the lens.

Despite the variety in shape, the peculiar variations we have identified as ESEs have in common a strong frequency dependence and are quite unlike the variations commonly observed in the light curves of compact extragalactic radio sources. ESEs identified at 2.7 GHz usually have no counterpart at 8.1 GHz, and in the one case where unusual variations do appear in the 8.1 GHz light curve (0954+658), the variations at the two frequencies are very dissimilar. Although the frequency coverage of ESEs has been minimal, the fractional deviation from the mean increases with increasing wavelength, but by an amount that varies from source to source. There is also the indication that the deviation above the mean is much more strongly frequency dependent than is the variation below the mean (0133+476 and 1749+096). Conversely, intrinsic variations that are usually attributed to the expansion of a region of relativistic plasma typically appear similar at, say, 2.7 and 8.1 GHz, except that the variations at 2.7 GHz are attenuated and lag behind those at 8.1 GHz. See Kellermann & Pauliny-Toth (1981) and the references contained therein.

A second, and generally weaker, contributor to variability at gigahertz frequencies is normal refractive interstellar scintillation (RISS). Interestingly the variability index of ESEs and RISS both increase with increasing wavelength (e.g., Rickett 1986). RISS and ESEs, however, are most dissimilar in their temporal behavior. Variations attributed to RISS appear as fluctuations with decorrelation timescales measured in days, or weeks, and persist over many years of observation. This is generally interpreted, in the case of extragalactic sources, to be the result of the proper motion of small-scale electron density turbulence in the ISM (e.g., Cordes, Weisberg, & Boriakoff 1985). The persistence of the fluctuations merely indicates the overall size of the turbulent region.

Many compact extragalactic radio sources flicker at gigahertz frequencies (Heeschen 1984; Simonetti, Cordes, & Heeschen 1985). Unlike observed ESEs, flickering usually occurs at

[1] Remote Sensing Division, Naval Research Laboratory, Code 7200, Washington, DC 20375.
[2] Center for Stochastic Processes in Science and Engineering, and Physics Department, Virginia Polytechnic Institute and State University, Blacksburg, VA 24061.
[3] Present address: National Radio Astronomy Observatory, Edgemont Road, Charlottesville, VA 22903.

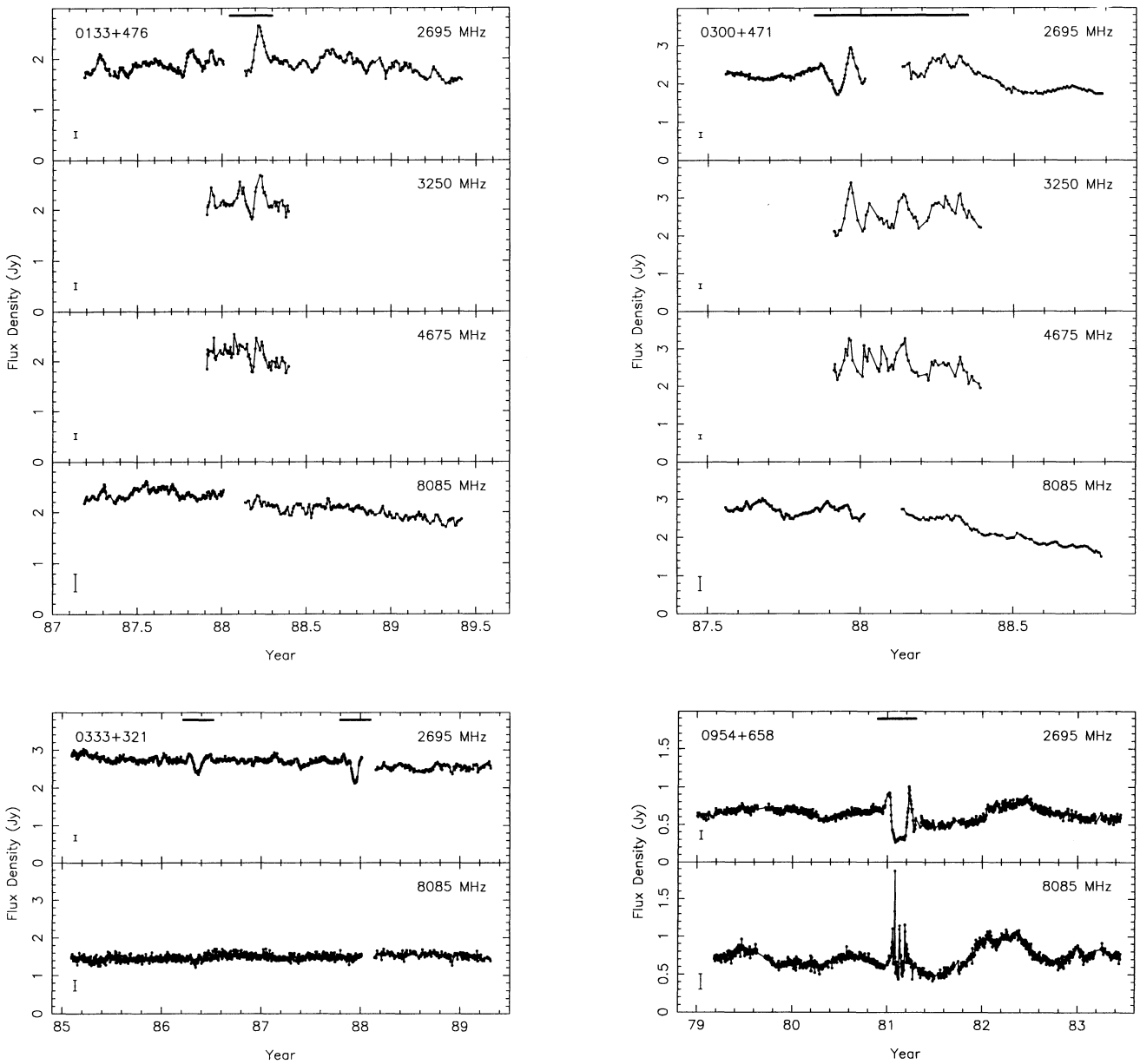

FIG. 1.—Radio frequency light curves of nine quasars that show evidence for extreme scattering events. The variations associated with ESEs are clearly atypical of the variations normally observed in these sources. Error bars are 3 σ in height and the time frame for each ESE is indicated by a bold horizontal line in the panel corresponding to the 2.7 GHz (2695 MHz) light curve. Except for 0954+658, the 8.1 GHz (8095 MHz) light curves have been smoothed using a 5 day boxcar algorithm to reduce the daily noise level, indicated by the error bar, and to see whether the unusual variations at lower frequencies have any weak counterpart at 8.1 GHz.

the several percent level and is persistent in any given source. Flickering is probably RISS, caused by continual motion of electron density turbulence across the line of sight (Rickett 1986). Conversely, ESE variations are smooth, much less erratic than flicker, and are evident over a clearly defined time interval, typically a few months.

We suggested in Fiedler et al. (1987a) that unusually strong refractive effects occurring in localized structures in the ISM are responsible for ESEs. Here we will expand upon that suggestion to include the effects of a general statistical redistribution of ray paths by a localized, inhomogeneous plasma structure. Romani (1988) has proposed that the most plausible scenario for strong lensing in the ISM occurs for lines of sight through the edge of a Galactic outflow, such as a supernova remnant, and Clegg, Chernoff, & Cordes (1988) have shown that ionized shock fronts viewed edge-on create strong refraction effects at radio frequencies. This edge-on geometry effectively relaxes the constraint on the required magnitude for electron density fluctuations from 1000 cm^{-3}, for a spherical lens, to 100 cm^{-3}, for a lens with an aspect ratio of 10:1. Even with the smaller of the two density estimates, the lenses are still overpressured with respect to the ambient ISM. Possible associations between the ESEs observed in the light curves of NRAO 140, 0954+658, and 2352+495 and specific Galactic structures are presented in Fiedler et al. (1993b).

In this paper, we present a model that relies on a statistical

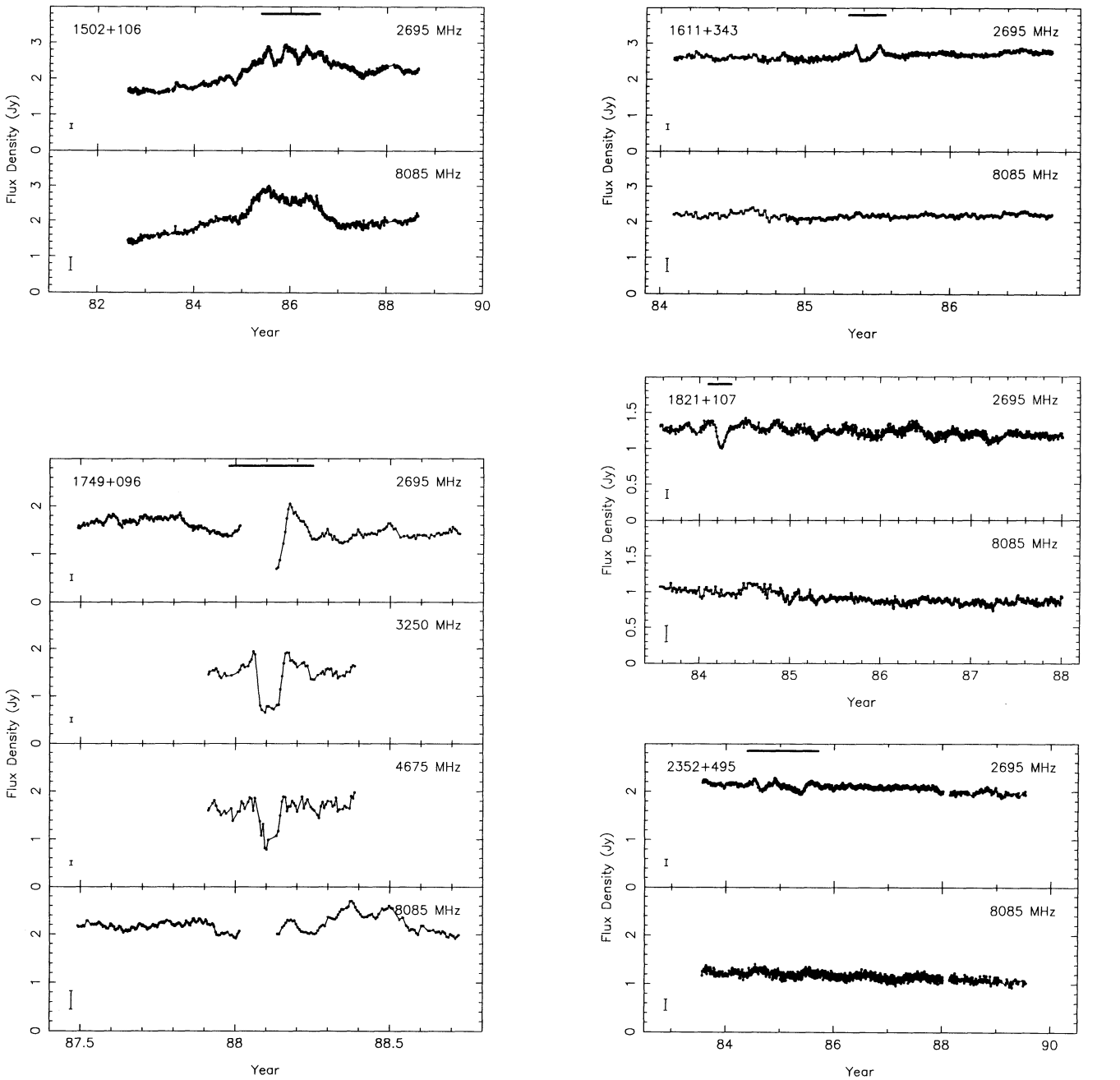

FIG. 1—*continued*

approach to simulate the distribution of flux density in the observer's plane. We assume that a localized region, referred to as the lens, contains electron density fluctuations that cause an angular broadening of the ray bundles arriving from a background radio source. The angle through which the rays are dispersed will be referred to as the broadening angle. The ray path broadening may be ude to diffraction from small-scale electron density turbulence in the lens; alternatively, the broadening may be caused by a statistically large number of refractions by a large number of electron density "clumps" within the lens. The exact cause of the broadening is not important at this point because we are merely presenting a conceptual model for the analysis of ESEs. We are able to reproduce the variety of shapes of ESEs below 8.1 GHz. The model depends on the projected two-dimensional geometry of the lens, the relative angular size of the lens with respect to the background source, and the relative angular extent of the broadening angle to the size of the lens. In the discussion of our observational results, we make a qualitative connection between these parameters and the observed shapes of events. The model is intended to provide a conceptual framework so that the discussion of the varied event shapes can be placed in a context useful for comparison with other ESE models (e.g., Romani et al. 1987).

At this early phase in the study of ESEs one must be careful not to interpret the timescales and amplitudes of the few events

presented in this paper as representative, or typical, of ESEs. It is possible that more ESEs are present in our light-curve data than we currently suspect. Identification is naturally more difficult when the peak-to-peak variation and timescale of an ESE is comparable to other sources of variability. Short-timescale and small-amplitude ESEs may be confused with RISS and, similarly, long-timescale and small-amplitude ESEs may be obscured by intrinsic variations. For the present, it is reasonable to assume that event amplitudes and timescales fall in a continuous range that merges with both RISS and intrinsic fluctuations. In this regard, the connection (if any) between lenses and the turbulent gas responsible for RISS is unclear. Because of the singular nature of ESEs, for the present we regard the corresponding lenses as discrete ionized regions. Also uncertain is the relationship (if any) between lenses and the AU-scale structure in H I reported by Dieter, Welch, & Romney (1976) and Diamond et al. (1989).

Improvements in our understanding of the physical conditions of the lenses themselves will have to wait until high-resolution and multifrequency observations are obtained during and after the next large ESE. The monitoring program conducted with the Green Bank interferometer will act as the trigger for these more detailed observations.

2. MONITORING PROGRAMS

The Green Bank interferometer (GBI) and the 300 foot diameter radio telescope, operated by the National Radio Astronomy Observatory,[4] were both used in monitoring programs of compact extragalactic radio sources in which ESEs were found. The GBI has been operated by the NRAO since the fall of 1978 for the US Naval Observatory and the Naval Research Laboratory as part of a joint program to study the Earth's polar motion (1978 October–1988 January). A transition in the use of the interferometer occurred in early 1988, when the polar motion observing program was replaced by one designed to search for more ESEs (1988 February–present).

The source list of the GBI program during the polar motion study varied considerably, but averaged about 25 sources observed every day, or every other day, for 9 yr (Fiedler et al. 1987b; Waltman et al. 1991). The second, and continuing, phase of the GBI program has a source list of approximately 150 compact extragalactic radio sources that were selected from the Preston et al. (1985) 2.3 GHz VLBI survey. The observing frequencies were 2.695 and 8.085 GHz for the period ending in 1989 August. A receiver upgrade in the fall of 1989 changed the observing frequencies to 2.25 and 8.3 GHz.

The transition in the operational objective of the GBI monitoring program occurred near the middle of our six month observing program (1987 December–1988 May) using the NRAO 300 foot radio telescope. Approximately 330 sources, also chosen from the Preston et al. (1985) survey, were observed every other day at 3.25 and 4.675 GHz with this instrument. A detailed discussion of these observations is given by Fiedler et al. (1993a). As of 1989 August, both monitoring programs combined resulted in a total of 594 independent source-years of observation. The overall coverage on the sky was a maximum at Galactic latitudes of 30°–45° (see Fig. 2*a*). The minimum at 0° extending toward 30° is a result of both a paucity of identified extragalactic objects near the plane of the Galaxy and the limitations imposed by Earth-based observations from the northern hemisphere (see also § 5 and Fig. 4). Although a substantial number of source-years have been observed, we point out that roughly 60% of the sources in the combined lists of the GBI and 300 foot monitoring programs were observed for a total duration of just under one-half of a year. These were sources observed as part of the 300 foot monitoring program that could not also fit into the regular GBI monitoring program. The linear-logarithmic plot in Figure 2*b* illustrates the number distribution of sources observed from 0.5 to 11 years.

Three ESEs were observed during the 6 month 300 foot monitoring program. They were also observed by the GBI. The ESEs occurred in the light curves of 0133+476, 0300+470, and 1749+096 (see Fig. 1). Unfortunately, these events occurred around the time when the interferometer was switching over to the new program, so there was incomplete time coverage of the 2.7 and 8.1 GHz data. Equally unfortunate was the failure of the lateral focus drive on the 300 foot radio telescope during the onset of the 0133+476 and 1749+096 events. This mechanical problem manifested itself as a sudden decrease in antenna temperature for all sources below 60° declination. The calibration procedure, discussed in Fiedler et al. (1993a), successfully removed the effects of the hardware failure from the radio light curves, but not in time to initiate VLBI observations while the events were going on. In summary, both instruments were functioning correctly during portions of both events, and when one instrument was down for maintenance the other was fully operational. We were therefore able to obtain simultaneous, or nearly simultaneous, independent observations of three ESEs at 2.7, 3.3, 4.7, and 8.1 GHz. This was the first time that ESEs were observed with an instrument other than the GBI.

3. STATISTICAL MODEL FOR FLUX REDISTRIBUTION

Any discussion of the shapes and frequency dependences of ESEs is more useful if given within the context of a model. From a cursory examination of Figure 1, one can see that a satisfactory model must be able to reproduce the varied shapes of ESEs. In this section we demonstrate the capabilities of the statistical approach to modeling ESEs. The model presented here assumes that the lens may be approximated by a screen, where the broadening angle, the size of the background source and the screen itself are all of comparable angular extent. The basic function of the screen is to broaden the angular distribution of rays from a background source. The exact method of how the broadening is accomplished is not important at this stage, where we are simply proposing a conceptual model. The broadening may occur by diffraction from small-scale electron density structure within the lens. Alternatively, the same result could be accomplished by refraction by a statistically large number of individual clumps within the lens. One difference between the two models (discussed more fully in the discussion section) is the required amplitude of the electron density fluctuations. Otherwise, the optics of the two methods is the same and the end result, vis-à-vis our statistical model, is the same.

A localized plasma structure with a smooth profile in the excess electron density (such as the Romani et al. 1987 model) will produce caustic surfaces that an observer will perceive as maxima in the corresponding light curve, whereas in our model the caustic structures are de-emphasized due to angular broadening of the ray paths, but enhancements in the background source flux density are produced by edge effects. Of

[4] The National Radio Astronomy Observatory is operated by Associated Universities, Inc., under contract to the National Science Foundation.

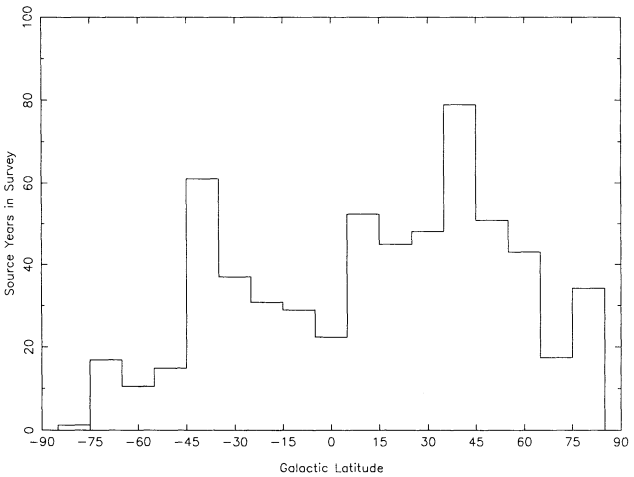

FIG. 2a

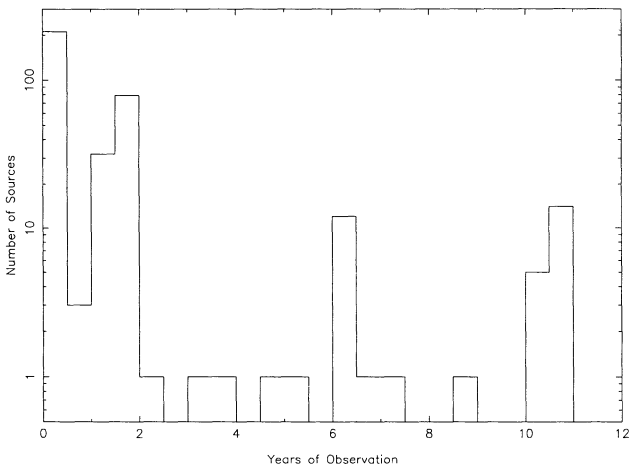

FIG. 2b

FIG. 2.—Histogram of (*a*) the number of source-years of observation distributed in Galactic latitude taken from surveys using the Green Bank interferometer and the NRAO 300 foot diameter antenna and (*b*) the number distribution of sources observed for different durations. Notice that in (*b*) the number of sources is plotted logarithmically. These distributions are the result of monitoring a total of 42 sources in a 9 yr period using the GBI, 149 sources in a 2 yr period, also using the GBI, and finally 328 sources over a 6 month period using the NRAO 300 foot diameter antenna.

particular interest is the possibility of simulating light-curve variations similar to the observed 2.7 GHz variations with, or without, significant variations at 8.1 GHz. In view of the increased number of ESEs observed over the past few years, the Romani et al. (1987) approach needs to be more carefully explored for comparison with observations and the statistical model presented here.

Although little is directly known of the structures in the ISM responsible for ESEs, there is some evidence to indicate that Romani's (1988) suggestion of an association with outflow in the ISM may be correct. The evidence presented in § 5 shows a coincidence between Galactic shell (or loop) structures and ESEs. A relatively large path length through an ionized structure seen edge-on in the limb of an expanding shell may be the requirement to produce large refraction angles, evidently necessary for an ESE to occur. The ionized structure might comprise a number of loosely connected sheets, filaments, or shock fronts distributed along the line of sight through the limb.

The issue of the magnitude of the refraction angles and the electron densities implied for ESE-producing structures is at present based on the tentative VLBI size of 0954+658 (Pearson & Readhead 1981), which sets an angular scale on the order of a milliarcsecond for the broadening angle that drives ESE variations. More recent VLBI observations of 0954+658 and other ESE sources will enable us to refine these parameters (Fey, Clegg, & Fiedler 1994).

For the purposes of introducing the basic model, we adopt a band-shaped lens as projected on the sky (see Fig. 5). This geometry is consistent with an edge-on view through a nearly planar lens. Other geometries are discussed below. We present some simple empirical rules for associating the specific features in the shape of an ESE with the relative angular sizes of the source angle θ_s, lens angle θ_l, and broadening angle θ_b. Here, θ_l is the width of the band-shaped lens. The proper motion of the lens across the background source is assumed to be along the small axis of the band. The source brightness distribution is assumed to be Gaussian with a full width at half-maximum (FWHM) of θ_s.

For a point source, electron density inhomogeneities throughout the lens are assumed to redistribute radiation randomly over a range of angles characterized by the angular width θ_b. As we pointed out in the beginning of this section, this could occur via both diffractive and refractive effects due to inhomogeneities on various scales within the lens. If these lenses are indeed associated with shock phenomena, as suggested by Romani (1988) and by Clegg et al. (1988), then they may be quite turbulent over a range of scales, possibly extending up to the scale size of the lens itself. This is the basic premise for the general statistical model we are proposing to describe ESEs.

In this model we represent the broadening of ray bundles as a Gaussian function with a FWHM of θ_b. For diffractive scattering, this is usually a reasonable approximation for the scattered intensity. Flux redistribution resulting from an ensemble of refractive material within the lens is also assumed to follow a Gaussian distribution. This distribution is regarded as representing the probability that any given ray is refracted through some angle. A consequence of the assumptions for the refractive case is that the flux density measured by the observer at any instant is a result of many rays from all points in the lens, as opposed to systematic focusing from individual clumps. Clearly, the angle θ_b depends upon the magnitude of the electron density inhomogeneities within the lens and can in general vary across it. For simplicity, we assume that θ_b is constant across the lens. In Appendix A, we demonstrate how a light curve is derived by integrating the redistributed radiation for all possible incidence angles due to a background source of finite angular size and combining this with the direct flux.

The critical components of an ESE are labeled in Figure 3*a*. The two light curves in Figure 3 are intended to illustrate the distinction in shape between cases where the lens is larger than the extent of the background source (Fig. 3*a*) and smaller than the background source (Fig. 3*b*). In Figure 3*b*, t_1 is at the origin. Notice that the x-axis represents an angular measure, in units of the source FWHM θ_s, and can be converted to a timescale if θ_s and the angular proper motion of the lens are known. For a Gaussian source-brightness distribution, the

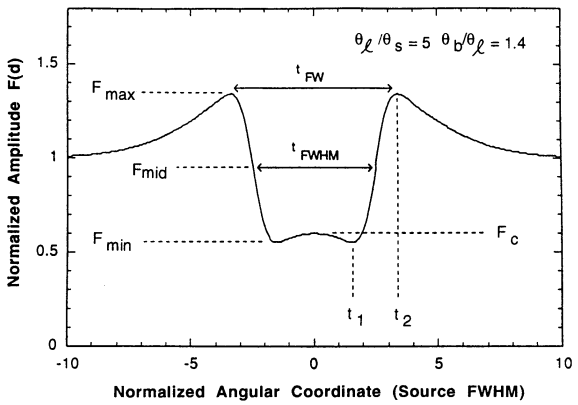

FIG. 3a

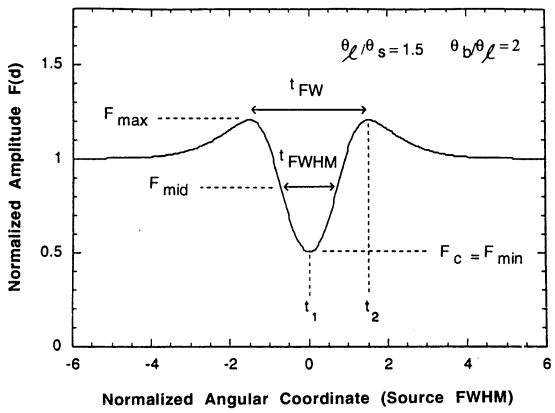

FIG. 3b

FIG. 3.—Model light curves of an ESE based on a band-shaped lens, where the size of the lens is (*a*) larger than the extent of the background source and (*b*) smaller than the background source. The components of an ESE are labeled. The ratios refer to the width θ_l of the lens, the FWHM θ_s of the background source, and the FWHM θ_b of the broadening function resulting from the electron density turbulence in the lens. The normalized amplitudes, $F(u_y)$, in (*a*) and (*b*) were obtained by evaluating eq. (A5) in Appendix A.

effective size of the source may be taken as roughly twice its FWHM. Therefore, the transition from an extended to a rounded minimum occurs as θ_l/θ_s decreases below about 2.

The consequences of the ratios θ_l/θ_s and θ_b/θ_l for the shape of an ESE can easily be seen. First, consider the extremes of these ratios. If the lens subtends a small fraction of the background source ($\theta_l/\theta_s \ll 1$), the amount of redistributed flux will be negligible compared to the total flux density. Detection of the resulting variations would then be limited by the sensitivity of the observation. Similarly, if the lens is extremely large in comparison to the background source ($\theta_l/\theta_s \gg 1$), the assumption of a constant broadening angle across the lens implies that there will be an equal amount of flux redistributed toward the observer as away. The net result is an absence of amplitude variations. The exception, of course, is when the edge of the lens transits the background source. Depending on θ_b/θ_l, large variations can result during such an edge crossing.

It is evident that the variations peculiar to this statistical model are simply the result of edge effects. The ratio θ_l/θ_s is a measure of how strongly the lens will interact with the background source, and θ_b/θ_l is related to the range of influence of either edge. The ray-broadening effects of opposite edges may overlap near the origin, or not at all, depending on the values of these ratios.

For example, a weak interaction between the lens and the background source occurs for a lens size less than the full width of the source ($\theta_l/\theta_s < 2$). The varying fraction of the source that is subtended by the lens during an event results in a shallow and rounded minimum. The details of the shape will be affected by θ_b/θ_l. Alternatively, for lenses larger than the source size, the minimum will be flat and deep if the broadening angle is constant across the lens and much larger than the lens ($\theta_b/\theta_l \gg 1$). If the extent of the broadening angle is on the order of the lens size, then a central peak in the minimum will occur. Allowing θ_b/θ_l to vary across the lens can result in a deep and rounded minimum. Finally, the fall and rise times between the minimum and bracketing maxima are closely related to the source size and the proper motion of the foreground lens.

So far, we have ignored the possibility of extended emission associated with the compact component undergoing extreme scattering. Because of this, the results presented above are most useful when expressed in a form that is independent of effects due to extended emission. The appropriate observable to describe the amplitude variations is

$$\Psi = (F_{\max} - F_0)/(F_0 - F_{\min}) , \quad (1)$$

where $F_{\max}$, $F_{\min}$, and F_0 are the maximum, minimum, and quiescent flux density levels, respectively.

Similarly, the most appropriate observable to describe the timescale of an ESE is, from Figure 3*a*,

$$\tau = t_{\rm FW}/t_{\rm FWHM} . \quad (2)$$

These observables may be used to obtain a model-dependent estimate of θ_b/θ_l and θ_l/θ_s. When combined with the fall/rise time, an estimate for the scale conversion from time to angular units can be used to determine the angular proper motion of the lens. The observables corresponding to the ESEs presented in the next section are listed in Table 1.

Interpretation of these dimensionless observables is complicated by numerous effects that are probably present, but not accounted for, in the simplified model for ESEs presented here. In addition to variable θ_b/θ_l across a lens, mentioned above, there is the geometry of the lens as projected on the sky. If the lens can be approximated as one-dimensional, i.e., if the long

TABLE 1

DIMENSIONLESS OBSERVABLES

	2.695 GHz		3.25 GHz		8.085 GHz	
SOURCE	Ψ	τ	Ψ	τ	Ψ	τ
0133+476	2.0	?	2	2	1	1.5
0300+470[a]	1.0	?	1	?	1	?
0333+321[b]	0.5	2.5	...	...	...	...
0954+658	0.8	1.2	...	...	...	...
1502+106	1.0	1.3	...	...	...	...
1611+343	>3.0?	1.5	...	...	...	...
1749+096	1.0	?	0.5	1.4	<0.2?	1.5
1821+107	0.3	1.5	...	...	...	...
2352+495	0.5	1.2	...	...	...	...

NOTE.—These values are only approximate, as they are affected by uncertainties in the estimate of the often variable baseline flux density level and by asymmetries in the shape of an ESE.

[a] Parameters correspond to the first large peak.

[b] Parameters correspond to the first of the two ESEs seen for this source.

axis of the lens is much larger than all relevant scale sizes in the problem, then the flux density will be conserved across the ESE. Otherwise, the flux density will not be conserved, indicating that the observable Ψ is geometry dependent. The best evidence for lens morphology will probably come from VLBI observations while an event is in progress.

Complex source and lens morphology as well as curvature in the lens proper motion, due to the Earth's orbital motion, will affect Ψ and τ and the overall symmetry of an ESE. There is also the possibility that proper motion will cause the background source to pass near, but not through, the lens, resulting in a single broad maximum having no associated minimum.

The frequency dependence of this model is addressed in the next section.

4. EXTREME SCATTERING EVENTS

Our observational results are summarized by the radio light curves illustrated in Figure 1. The 10 ESEs found to date are categorized below by their time and frequency dependence. Here we discuss the various shapes of ESEs within the framework of our statistical model.

4.1. 2.7 GHz *Time Dependence*

Figure 1 illustrates the wide variety in event shapes at 2.7 GHz and the striking absence of unusual variations at 8.1 GHz, with the exception of 0954+658. Some events appear as paired maxima surrounding an extended flat minimum, others as rounded minima with or without surrounding maxima, and some appear to occur in rapid succession.

4.1.1. *Flat Minimum*: 0954+658, 1611+343, *and* 1749+096

The statistical model implies that the flat minima in these cases are due to lens sizes greater than the angular size of the background source, $\theta_l/\theta_s \geq 2$, and that $\theta_b/\theta_l \geq 1.4$. More importantly, a flat minimum implies a fairly uniform distribution in θ_b across the lens. All three of these sources are highly compact at gigahertz frequencies.

Zensus, Procas, & Pauliny-Toth (1984) found that 73% of the 5 GHz flux density of 0954+658 resides in a barely resolved component with axial dimensions of 0.8 mas by less than 0.5 mas. Pearson & Readhead (1981) reported finding most of the 5 GHz flux density in a component 0.39 mas in size. The difference in these sizes is probably the result of model fitting to data sampled differently in the u-v plane and may be an indication of structure at the resolution limit.

The quasar 1611+343 (DA 406) is a low-frequency variable (Altschuler et al. 1984), with variability characteristics indicative of refractive scintillation (Dennison et al. 1984a). Romney et al. (1984) report that an unresolved structure ($\lesssim 3$ mas) contains at least 80% of the total flux density at 1.67 GHz.

The BL Lac object 1749+096 is known to have very little arcsecond-scale extended emission (Antonucci & Ulvestad 1985). At least 90% of its flux density resides in a 0.2 mas scale component (Weiler & Johnston 1980). This large percentage is consistent with the deep minimum and large peaks bracketing the ESE in this source.

At present it is unclear why the event in 1611+343 varied weakly in comparison with 0954+658 and 1749+096, despite the large fraction of total flux density contained within a milliarcsecond-scale size. One possibility is that the ESE involved a highly compact substructure containing only a moderate fraction ($\simeq 10\%$) of the total flux density. Clearly, a detailed understanding of the sub-milliarcsecond structure of these sources is required to accurately interpret these events and to deduce the ray-broadening and geometrical properties (θ_l/θ_s and θ_b/θ_l) of the intervening material. This may have to await the arrival of orbiting VLBI.

4.1.2. *Rounded Minimum*: 0133+476, 0333+321, *and* 1821+107

These sources and those listed in the next subsection all have an ESE with a rounded minimum in their 2.7 GHz light curves. Although we make a distinction between isolated events and multiple events, the lenses associated with these ESEs all contain lenses whose angular sizes are evidently smaller than the compact background quasar, or $\theta_l/\theta_s < 2$. We point out that, unlike the case for flat minimum where the depth of the minimum depends primarily on θ_b/θ_l and the relative fraction of the total flux density in the compact component, the depth of the rounded minimum strongly depends on these quantities and θ_l/θ_s.

We note that these conclusions rely on the assumption that the broadening angle is constant across the lens. If, for example, the magnitude of the broadening angle θ_b peaks at the center of the lens and decreases toward zero at its edge, then a flat minimum is no longer possible. Therefore, the presence of a flat minimum in an ESE, as mentioned earlier, may be used to argue for uniformity in the broadening angle, but a rounded minimum is not sufficient to make any unique conclusions about θ_l/θ_s, or the distribution of θ_b/θ_l across the lens.

The 2.7 GHz light curves of 0133+476 and 1821+107 are especially interesting because of the additional presence of persistent fluctuations that may be attributable to RISS. These light curves may represent instances of lenses embedded in regions of extended turbulence. Although the structures responsible for the ESE and RISS in the light curves of these sources may not be physically related, the presence of both effects with comparable peak-to-peak amplitudes could represent the domain where the conditions for RISS and ESEs begin to overlap.

Both 0133+476 ($z = 0.858$) and 1821+107, a BL Lac object, are highly compact. VLBI studies of 0133+476 over a range of frequencies report that nearly all of the flux resides in a single barely resolved component (Lawrence et al. 1985; Marscher & Schaffer 1980; Pearson & Readhead 1988; Zensus et al. 1984). At 5 GHz, Pearson & Readhead report that more than 89% of the total flux density is in a 0.9×1.4 mas component.

Despite the limited time coverage of the 2.7 GHz ESE in 0133+476, the event minimum appears to extend only slightly below the quiescent level, whereas the maximum is well in excess of it. Our statistical model suggests, for an observer who views the background source as traversing a diameter of a two-dimensional lens, that the height of the maximum above the quiescent level be less than or equal to the depth of the minimum. This could imply that the proper motion of the lens caused 0133+476 to cross a chord, rather than a diameter, and thereby avoid the area where the greatest amount of flux is redistributed away from the observer. Such a model would assume that the broadening has a two-dimensional lens as discussed above.

The 2.7 GHz light curve of the superluminal source 0333+321 (NRAO 140, $z = 1.26$) contains the only clear example of two events separated in time (1.7 yr) by a margin much greater than the duration of each event (0.1 yr). We also point out that 0333+321 varies strongly at low frequencies (Dennison et al. 1984b).

Although the VLBI structure at 1.67 GHz of 0333+321

(Marscher et al. 1987) reveals a complex jet, it appears unlikely that the two events in the light curve of this source were caused by a single lens crossing the source. The proper motion of the lens spans roughly 3 times the angular extent of the complex structure of NRAO 140 over the 1.7 yr interval separating the two events. This suggests that two lenses produced the two ESEs. We have assumed that the lens is at the distance of the Perseus cloud complex (Fiedler et al. 1993b) and have included the effects of solar motion, Earth orbital motion, and differential Galactic rotation. The general trend in the proper motion is roughly along the line joining the individual radio components. Including a peculiar motion that corresponds to an outflow through the foreground of NRAO 140 increases the discrepancy even further.

Marscher (1988) has reported a remarkable change in X-ray absorption, implying a column density change from 6×10^{21} cm^{-2} in 1980 to about 2×10^{21} cm^{-2} in 1985. These rapid changes suggest the existence of strong transverse gradients in the column density of neutral gas on quite small scale sizes in the ISM. The apparent column density fluctuations are about a factor of 10^5 larger than those we inferred for the ionized gas causing the ESE seen in 0954+658.

4.1.3. *Multiple Events*: 0300+470, 1502+106, *and* 2352+595

The unusual variations in the 2.7 GHz light curves of these sources satisfy the basic criteria for ESEs outlined in § 1. That is, the variations were transient and atypical of those normally observed in these sources. Also, similar variations were not observed at 8.1 GHz. Note that these ESEs appear to span up to about 1 yr, rather than the few month timescale typical of the other ESEs identified so far.

The variations in the light curves of 0300+470 and 1502+106 appear to be three closely spaced events, whereas for 2352+595 the variations appear as two events. One likely cause for multiple events is a multicomponent structure in the background source, or clumpiness in the turbulent electron density distribution defining the lens, or both. The event in the light curve of 0300+470 is particularly interesting because the first minimum is not preceded by a steep maximum, but is followed by one. This event shape can occur when the edge of a very large lens crosses through the observer's line of sight to the background quasar.

Unlike the ESE in 0300+470, the event in the light curve of 1502+106 appears to be a series of minima bracketed by maxima. This pattern is consistent with a separation distance that is on the order of the clump size in a complex source or lens distribution. Inspection of Figure 1 shows that the ESE in 1502+106 occurred during a flare that was probably intrinsic to the source. This apparent coincidence may have relevance for the likelihood of observing an ESE. Two conditions must be met to produce an ESE. First, there must be a compact background source, and, second, unusually strong electron density fluctuations must be present in a foreground Galactic object. Some sources may not have sufficiently compact structures, or the fractional flux density in the compact component may be too small to produce a noticeable ESE. However, if such a source flares, the evolving compact flare component could represent a sizeable fraction of the total flux density of the source and thereby increase the likelihood of an ESE.

It is tempting to associate the multiple variations of the ESEs in 0300+470 and 1502+106 with complex structure in the ISM such as a shock wave, its precursors, or its cooling substructure. This is because both of these sources are highly compact (Antonucci & Ulvestad 1985; Lawrence et al. 1985; Weiler & Johnston 1980; Zensus et al. 1984). Although good maps at these frequencies are apparently unavailable at present, it appears that in both cases most of the flux density originates in sub-milliarcsecond size scales. Alternatively, however, complex substructure in the morphologies of these sources may be responsible for the repetitive nature of the events.

Another possible mechanism for producing multiple events may be illustrated by considering the case of 1502+106, where the two ESE minima are separated by roughly 0.5 yr. Although two closely spaced lenses, each having a transverse velocity well in excess of the Earth's orbital motion, could have produced the observed events, we note that a single lens could, in principle, produce the same result via parallax. For example, if the foreground lens were at a distance of 1 kpc and if its peculiar motion were roughly parallel to the solar motion as projected on the sky, then retrograde motion can carry the lens in front of 1502+106 more than once. There will be two crossings separated by roughly 0.5 yr if the peculiar velocity of the lens is around 5 or 27 km s^{-1} in the indicated direction. These complementary solutions, at 5 and 27 km s^{-1}, occur near cusps in the proper motion of the lens. The former corresponds to a "looping" proper motion extended toward the southwest and the latter to the motion reversed toward the northeast. As in the case of 0333+321, we have included the effects of Galactic rotation, Earth orbital motion, and solar motion.

A third possibility for the two events in 1502+106 is that a single lens had passed in front of two compact components separated by $\lesssim 1$ mas. Again, by exploring possibilities in proper motion we find that there is a wide range in component orientation and lens-peculiar motion that will satisfy this latest possibility. However, there are several possible caveats that should be mentioned for this case. The compactness of 1502+106 was inferred primarily from VLBI observations at 5 GHz (Zensus et al. 1984). It is possible that at 2.7 GHz two or more components are present with a separation of several milliarcseconds. Similar arguments apply to 0300+470, although the compact flux density distribution is not well constrained in this case (Weiler & Johnston 1980). Clearly, better VLBI observations of these sources are needed.

Unfortunately, based on observational evidence, none of these three possibilities may be ruled out as an explanation for the apparent multiple ESE in the light curve of 1502+106.

The quasar 2352+495 has been mapped at 5 GHz (Pearson & Readhead 1988) and has complex structure around a compact component (0.9 mas FWHM) comprising about three-quarters of the total flux density. Most of the remaining flux density in the map lies within several milliarcseconds of the most compact component.

If the shape of the ESE is attributed to intrinsic source structure, then the inferred proper motion of the lens is $\lesssim 3$ mas yr^{-1}. As before, this proper motion translates to a relative velocity smaller than the Earth's orbital velocity, assuming the lens is not much farther than 1 kpc. Interestingly, the shape of the ESE in the 2.7 GHz light curve need not be a result of complex structure in the source or lens. If the lens has an angular size greater than that of the source ($\theta_l/\theta_s > 2$) and the broadening angle is roughly equal to the size of the lens ($\theta_b/\theta_l \simeq 1$), then our statistical model predicts a peak in the middle of an otherwise flat minimum, as observed. This possibility is compatible with the radio map as long as the lens is

larger than about twice the source extent, or about 4 mas. In this case, the proper motion is $\simeq 6$ mas yr^{-1}, which gives a transverse velocity of $\simeq 30$ km s^{-1} at a distance of 1 kpc. Because of the more reasonable proper motion, we prefer this latter explanation for the shape of the ESE in 2352+495.

4.2. 8.1 GHz *Time Dependence*

The most striking aspect of ESEs is the absence of unusual variations at 8.1 GHz despite the large, in some cases 50%, variations observed at 2.7 GHz. Equally striking is the one exception, 0954+658, which shows four strong spikes at 8.1 GHz, simultaneous with the ESE observed at 2.7 GHz. The duration of each of these spikes is about 10 days (see Fig. 1).

We suggested in Fiedler et al. (1987a) that the spikes may be due to strong refractive focusing by the lens. In this case, the refraction angles are comparable with the angular spacing between clumps, so that, in effect, this angular scale has a focal length comparable with the distance to the lens. Additionally, the background source must have compact structure on scales not significantly in excess of the refraction angles. At 2.7 GHz, the refraction angles are larger by a factor of 9, in which case the lens redistributes flux in the statistical manner described by our model. The main difference between our refractive focusing model for the spikes and the caustic model of Romani et al. (1987) is that in our model the occurrence of spikes is rare, because of the requirements set forth above. The caustic surfaces in our model are smeared out and de-emphasized due to ray broadening, whereas the caustics in the Romani et al. model remain sharp and easily observed.

Although we find no other clearly identifiable ESEs in the 8.1 GHz data, there are weak features in a few of the 8.1 GHz light curves that appear suspicious. These features contain local minima and maxima that occur at the same time as those in the ESEs found at lower frequencies. Although these weak variations may be coincidental, being related to either RISS or intrinsic effects, nevertheless they may be found at 8.1 GHz in 0133+476 following the gap in the data, in 0300+470 preceding the gap in the data, in 0333+321 during the first event, and possibly even in 2352+495.

4.3. *Frequency Dependence*

For the sources 0133+476, 0300+470, and 1749+096 we have reasonably good frequency coverage, despite some unfortunate gaps in the light curves, especially at 8.1 GHz. First, we note that there is a general trend for the peak-to-peak amplitudes and the overall widths of these events to decrease with increasing frequency as expected.

As noted earlier, the rounded minimum of 0133+476 suggests that $\theta_l/\theta_s \leq 2$. Recall that $2\theta_s$ represents the full width of the background source. Since the source size is likely to vary with frequency, so then does the ratio θ_l/θ_s. We point out that the source size is the size "seen" by the lens. It will depend on intrinsic effects and possibly on scattering by electron density inhomogeneities located beyond the structure causing the ESE. For the purposes of the present discussion we will assume $\theta_s \propto \nu^{-1}$. We therefore expect the ratio θ_l/θ_s to vary in proportion to the frequency.

Because the source represents a smaller fraction of the lens as the frequency increases and because we can expect the broadening angle θ_b to decrease even more rapidly with frequency ($\theta_b \propto \nu^{-2}$), the overall duration of an ESE is also expected to decrease. The decrease in the fall/rise time, $t_2 - t_1$ (see Fig. 3*a*), is due primarily to the changing source size, whereas the duration of the wings of the ESE is governed by the broadening angle θ_b. The proportional change in duration of an ESE is expected to be larger when $\theta_l/\theta_s \leq 2$, as in 0133+476, since the source, rather than the lens, dominates the duration of the ESE in this limit.

Similarly, as the angular extent over which flux is redistributed decreases, departures in the light curve away from the quiescent level are also expected to decrease. The broadening angles referenced to the angle at 2.7 GHz for the other three observing frequencies are estimated to be $\theta_b(3.3)/\theta_b(2.7) \simeq 2/3$, $\theta_b(4.7)/\theta_b(2.7) \simeq 1/3$, and $\theta_b(8.1)/\theta_b(2.7) \simeq 1/9$. Very little ray broadening is expected at 8.1 GHz, consistent with our observations.

The multiple ESE in 0300+470 is evidently a result of complex structure in the foreground lens. Notice that the rise toward maximum occurring around 1987.9–1987.95 at 3.3 GHz is larger than at 2.7 GHz. However, if the peak-to-peak variation is normalized by the quiescent flux density level, estimated by the midpoint of the rise, we find that the variations are the same at both frequencies. In fact, we find no obvious frequency dependence between the 2.7 and 3.3 GHz light curves on either side of the gap in the 2.7 GHz data.

At 4.7 GHz the variations do appear to diminish slightly, but not to the degree observed for the ESE in 0133+476. Interestingly, there is some marginal evidence for extreme ray path disturbances at 8.1 GHz. The successive maxima and minima spanning 1987.85–1988.0 at 2.7 GHz coincide with weak local maxima and minima at 8.1 GHz.

In view of our statistical model, the gradual frequency dependence together with the unique shape of the ESE in 0300+470 imply a specific morphology for the lens. Although we mentioned earlier that crossing the edge of a large lens, where $\theta_b/\theta_l \ll 1$, can produce an ESE with no leading maximum, this geometry is unlikely because the amplitude variations are very sensitive to changes in θ_b.

The weak frequency dependence and rounded minima are consistent with $\theta_l/\theta_s \leq 2$. In this regime the amplitude of the maxima of an ESE are predicted to be fairly constant over a wide range in broadening angles, provided that $\theta_b/\theta_l \geq 2$. For example, the values of θ_b/θ_l at the four frequencies may be roughly 4.5, 3, 1.5, and 1 as the frequency increases to 8.1 GHz. Below $\theta_b/\theta_l \simeq 2$ the amplitude decreases rapidly toward the quiescent flux density level. Similar comments can be made about the depth of the minimum. The slight rise in flux density preceding the first minimum at 2.7 GHz is easily accounted for if a gradient in θ_b is assumed; i.e., θ_b monotonically increases as the initial substructure of the lens passes through the observer's line of sight to 0300+470. The subsequent variations in the ESE are probably due to additional substructures, also $\theta_l/\theta_s \leq 2$, spaced roughly $2\theta_s$ or less apart.

The ESE in 1749+096 appears to follow the same general behavior as the one in 0133+476, as the amplitude of the maxima and the depth of the minimum both decrease with increasing frequency. If the minima at 3.3 and 4.7 GHz are taken as flat-bottomed, and by implication the minimum at 2.7 GHz would also be flat-bottomed, then the event in 1749+096 probably has a larger relative lens than the event in 0133+476, namely, $\theta_l/\theta_s > 2$ at these three frequencies.

From equation (1) and the model dependence of Ψ on τ we find that for decreasing θ_b/θ_l, or increasing frequency, the height of the bracketing peaks above the quiescent level should

become a substantial fraction of the depth of the minimum. This is contrary to observations of the 4.7 GHz ESE in 1749+096. Bracketing peaks are not observed despite the presence of a substantial minimum. Whether this is true for the 4.7 GHz event in 0133+476 is difficult to tell, since the quiescent level of the source evidently changed during the event.

However, if peaks are present in the 1749+096 event, but hidden in the noise, then we would expect $\theta_b/\theta_t \geq 5$ at 4.7 GHz, assuming, by inspection of the light curve, that $\Psi \leq 0.2$. One consequence of such a large θ_b/θ_t is that the depth of the minimum is not expected to change appreciably as the broadening angle increases corresponding to a decrease in frequency to 2.7 GHz. This is contrary to the observed variation in the depth of the minimum with frequency.

Our concern over the apparent absence of maxima bracketing the ESE at 4.7 GHz in 1749+096 should be tempered by the fact that we have a small baseline in the light curve on either side of the ESE. It is possible, although not convincing, that there are significant peaks, of comparable widths to those in the 3.3 GHz light curve, that are heavily corrupted by noise.

Finally, if the peaks are truly absent at 4.7 GHz, then one avenue to explore in a search of the missing flux density would be to consider anisotropic flux redistribution. That is, anisotropic ray broadening that is frequency dependent—weakly anisotropic at 2.7 GHz and strongly anisotropic at 4.7 GHz and above, in the case of 1749+096. The flux that would have otherwise produced a maximum has been redistributed in directions other than along the observer's path through the image cast by the lens. Judging from the observations of extragalactic sources scattered by the interplanetary medium (e.g., Narayan, Anantharamaiah, & Cornwell 1989; Armstrong et al. 1990) and the modeling by Higdon (1984) of anisotropic magnetogasdynamic turbulence, one would expect that if ESEs are associated with shocked regions, where planar symmetry has been introduced to the local magnetic field distribution, anisotropic ray broadening could play a significant role in the interpretation of lensing in the ISM.

5. SPATIAL DISTRIBUTION AND RATE OF ESEs

Positions of the 365 sources from the combined lists of our two monitoring programs are plotted in Figure 4. The stars indicate the positions of the nine sources exhibiting one or more ESEs. Also shown are the four major Galactic continuum loops (Berkhuijsen, Haslam, & Salter 1971). A possible association of event sources with the foreground loops is evident, as first suggested by Romani (1988). Also, the event sources appear to be grouped in the North Polar Spur associated with Loop I, and in a 20° × 10° region along Loops II and III just below the plane near the Galactic anticenter. The source which showed the strongest event, 0954+658, is located near the northern extreme of Loop III.

To test for a possible association between loops and event source we rank-ordered all compact sources monitored according to their angular distances from the nearest loop (with rank 1 assigned to the source closest to a loop). We used the center coordinates and radii of the four loops given by Berkhuijsen et al. (1971). Our compactness criterion required that a source have a fringe visibility of at least 0.30 or a correlated flux of at least 430 mJy in the VLBI survey of Preston et al. (1985), for which the fringe spacing was about 3 mas at 2.3 GHz. This criterion encompasses all nine event sources and insures that the other sources in the sample are sufficiently compact to show an ESE. There are 211 sources satisfying the compactness criterion. The sum of the ranks of the nine event sources was used as the test statistic W and found to be 479. Under the null hypothesis, in which the event sources have no relationship with the loops, the expectation and standard deviation of W in this case are $\langle W \rangle = 954$ and $\sigma_W = 179$ (see Appendix B). For large overall sample size the distribution of W is nearly Gaussian, and we find that the measured value of W differs from that expected on the basis of the null hypothesis by 2.65 σ. For a one-sided test (i.e., we suspect that the event sources are preferentially *close* to the loops), we would expect to find a value of $W \leq 479$ in 0.4% of a large number of cases.

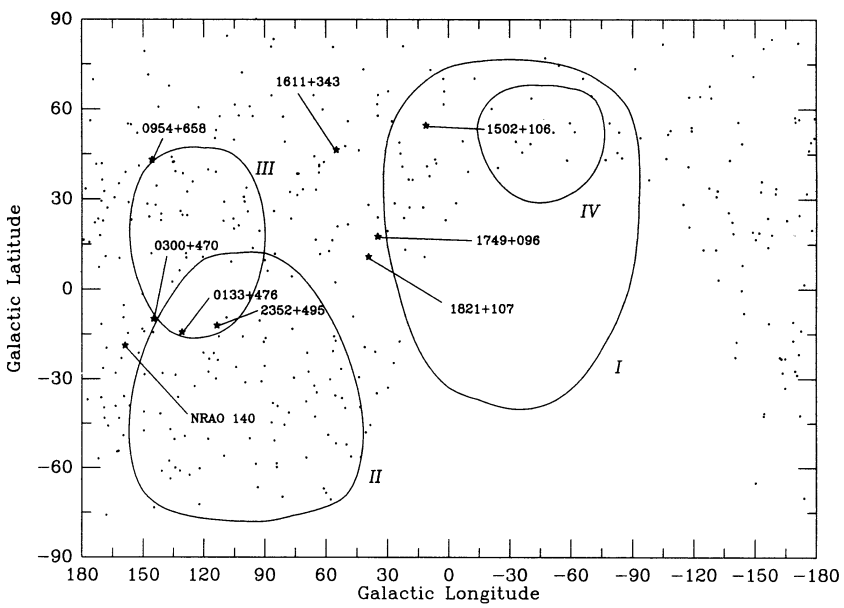

FIG. 4.—Angular distribution, in Galactic coordinates, of sources observed by our monitoring programs. Those sources that have an ESE in their light curve are labeled, and the loops represent the four most prominent large-scale continuum loops in the Galaxy.

To test this, we ran 10,000 computer simulations, in each of which the sky north of $-18°$ declination was randomly populated with 211 sources. Nine sources were then randomly selected and designated as event sources. The entire source population was rank-ordered as described above, and W was computed by summing the ranks of the nine designated source events. The resulting distribution of W over 10,000 simulations was found to be consistent with Gaussian. Values of $W \leq 479$ resulted in 33 cases. This is consistent with the number expected from Gaussian statistics (~ 40) and confirms the estimated probability (0.4%) that the apparent association between event sources and loops is a random occurrence.

Because the event sources were all monitored for periods of at least 2.42 yr, the majority of the sources in the sample, being monitored for 0.48 yr in the 300 foot program, are less likely to show any events. Therefore, we eliminated all sources monitored for less than 2.4 yr, leaving a total of 30 sources, and repeated the analysis. In this case, we found $W = 88$ as compared with an expected value of 139.5 and $\sigma_W = 22.1$, giving a deviation from the expected value of 2.33 σ. This indicates that the null hypothesis, if true, yields such a result in 1% of cases. This was confirmed by running 10,000 simulations. Values of $W \leq 88$ occurred in 102 cases, consistent with the expected number. As in the previous case, the distribution of W was found to be Gaussian with the predicted mean and standard deviation.

Several additional tests were carried out to eliminate the possibility that this correlation might be the result of some other correlation in the data. We tested the subpopulation of sources monitored for long periods of time (> 2.40 yr) for proximity to the loops, using the same method, and found no significant correlation. (Of course, as we have shown, even within this subpopulation the event sources lie preferentially closer to the loops at the 99% confidence level.) We also varied the coordinates and radii of the loops within the error estimates given by Berkhuijsen et al. (1971) and found relatively little change in W.

We conclude, therefore, that compact sources with small angular separations from major loops in the Galactic foreground radio emission are more likely to exhibit ESEs than compact sources with large angular separations from the loops. The probability that the correlation we have observed is a chance occurrence is about 1 in 100. Evidently, the loop structures provide the necessary conditions of enhanced electron density turbulence required for ESEs. The correlation with the circular outline of the loops strongly suggests an enhancement of diffractive or refractive effects along lines of sight nearly tangent to the spherical structures that constitute the loops. If these structures are outflows as seems likely, they may contain numerous small-scale structures such as shocks and secondary outflows. An ESE may be the result of an alignment between the long axis of quasi-continuous sheets or filaments and the observer's line of sight to a background compact source. The transverse angular dimension of these structures seen edge-on, inferred in Fiedler et al. (1987a), would be on the order of a few milliarcseconds.

Evidently, the distribution of ESE-producing structures along the loops may not be uniform, with the southern periphery of Loop III and the North Polar Spur having a greater density of these structures. The loops may also play a role in low-frequency variability (Shapirovskaya 1978).

The rate of occurrence of ESEs may be estimated by comparing the number of source-years spanned by all of the ESEs and the number of source-years observed in our two monitoring programs,

$$G = 4.8/594 \simeq 0.008 \text{ event-years per source-year} . \quad (3)$$

The 4.8 yr estimate corresponds to the total duration of the horizontal bars plotted in the 2.7 GHz panel in the light curves shown in Figure 1. Also, since we observed 10 ESEs in 594 source-years of monitoring, one can expect

$$H = 10/594 \simeq 0.017 \text{ events per source-year} , \quad (4)$$

or about two ESEs per year using our current GBI source list of 150 sources.

More important, equation (3) can be used to estimate the total number density of lenses on the sky. From the discussion of the statistical model, we interpret the angular width of a lens to correspond to $t_{\rm FWHM}$ and not the total duration of an event (see Fig. 3*a*). Since G is based on the total duration of the observed events, a correction factor, $\alpha \simeq 2$, is used to estimate the effective covering factor of lenses on the sky, G/α. The number density of lenses, $n_{\rm esc}$, can then be seen as

$$n_{\rm esc} \simeq \frac{G/\alpha}{\Omega_{\rm esc}} , \quad (5)$$

where $\Omega_{\rm esc}$ is the average solid angle subtended by an ESE-producing lens. The area $\Omega_{\rm esc}$ can be estimated by assuming a diameter of 5 mas (Fiedler et al. 1987a) and an axial ratio of β (> 1), or $\Omega_{\rm esc} \simeq 20\beta$ mas^2. Notice that equation (5) assumes that the lenses are uniformly distributed across the solid angle subtended by our monitoring programs. If the regions are confined to an area within 10° of a Galactic continuum loop, then equation (5) would increase by a factor of 1/0.44, corresponding to the reciprocal of the fraction of source-years observed within this area.

We estimate the number density of lenses to be

$$n_{\rm esc} \leq 200/\beta \text{ or } 450/\beta \text{ arcsec}^{-2} , \quad (6)$$

depending on whether the lenses are distributed over an area corresponding to the scope of our survey, or over an area within 10° of the Galactic continuum loops, respectively.

6. DISCUSSION

The statistical model presented here successfully explains the varied morphologies of ESEs, although their frequency dependence is less well understood. This model is a generalization of the one given in Fiedler et al. (1987a), in that it allows the flux redistribution to occur on diffractive or refractive scales, or on both. In this section we estimate the rms density fluctuation in an ESE-producing structure harboring a spectrum of irregularity scales. As an example, we consider a power-law spectrum of the form

$$P_{\delta n_e}(q) = C_n^2 q^{-\alpha}, \quad q_0 < q < q_i , \quad (7)$$

where q is the spatial wavenumber, $P_{\delta n_e}$ is the power spectrum of electron density irregularities over the range of outer and inner scales $l_0 = 2\pi/q_0$ and $l_i = 2\pi/q_i$, respectively, and the constant C_n^2 measures the strength of the fluctuations. For most situations in the ISM, the power-law index is ~ 4 (Rickett 1990).

An initially planar wave front emerges from the medium corrugated. For simplicity we consider refraction, which results

from transverse gradients imposed upon the wavefront. The refraction angle is

$$\bar{\theta}_r = \frac{\lambda}{2\pi} \nabla\varphi \,, \tag{8}$$

where φ is the emergent phase. The gradient is two-dimensional in a plane perpendicular to the line of sight; the overbar indicates a two-dimensional vector in this plane. The ensemble average of θ_r^2 is straightforwardly calculated to be

$$\langle\theta_r^2\rangle = \left(\frac{\lambda^2}{4\pi^2}\right) \iint dq_x\, dq_y\, q^2 P_\varphi(\bar{q}) \,. \tag{9}$$

The power spectrum of the emergent phase fluctuations, $P_\varphi(\bar{q})$, is related to that of the density fluctuations by

$$P_\varphi(\bar{q}) = 2\pi r_e^2 \lambda^2 Z P_{\delta n_e}(\bar{q},\, q_z = 0) \,, \tag{10}$$

where Z is the thickness of the medium, and r_e is the classical electron radius. For $\alpha = 4$, we find that

$$\langle\theta_r^2\rangle = r_e^2 \lambda^4 Z C_n^2 \ln \frac{q_f}{q_0} \,, \tag{11}$$

and

$$\langle\delta n_e^2\rangle = \iiint d^3\boldsymbol{q} P_{\delta n_e}(q) \simeq 4\pi C_n^2 q_0^{-1} \,. \tag{12}$$

Since we are considering just refraction in this example we have included only those spatial wavenumbers between q_0 and the Fresnel wavenumber, $q_f = 2\pi/(\lambda Z)^{1/2}$, in calculating $\langle\theta_r^2\rangle$.

We can now estimate the rms density fluctuation required to produce the rms broadening angle, since

$$\langle\delta n_e^2\rangle \simeq \frac{4\pi}{\ln(q_f/q_0)} \frac{\langle\theta_r^2\rangle}{r_e^2 \lambda^4 q_0 Z} \quad (\alpha = 4) \,. \tag{13}$$

We assume that the outer scale is set by the transverse dimension of the region; i.e., $q_0 \simeq 2\pi/L$, then $q_0 Z \simeq 2\pi h$, where h is the region's depth-to-width ratio. In the case of the event in 1749+096, our model predicts $\theta_l/\theta_s \simeq 6$ and $\theta_b/\theta_l \simeq 1.3$. Using a source size of 0.2 mas (Weiler & Johnston 1980) gives $\theta_l \simeq 1.2$ mas and $\langle\theta_r^2\rangle^{1/2} = \theta_b/[2(\ln 2)^{1/2}] \simeq 1.0$ mas. This gives $\langle\delta n_e^2\rangle^{1/2} \simeq 140$ cm$^{-3}/h$. In calculating the ratio $q_f/q_0 \simeq L/(\lambda r)^{1/2} \simeq \theta_l (r/\lambda)^{1/2}$, we have arbitrarily assumed a distance r of 500 pc, giving $q_f/q_0 \simeq 75$. The rms density fluctuation estimated above is of course highly insensitive to this ratio.

If the spectrum continues to scales smaller than the Fresnel scale, then diffractive scattering also will be present, and if $q_i \gg q_f$, then the diffractive scattering angle will be comparable to the refractive angle calculated above (Cordes, Pidwerbetsky, & Lovelace 1986). If $\alpha < 4$, then diffractive scattering will dominate over refractive broadening. If, on the other hand, $\alpha > 4$ and $q_0 \ll q_f$, then refractive broadening will dominate (Cordes et al. 1986). Yet another possibility is that the density fluctuations are confined to scales larger than the Fresnel scales ($q_i \ll q_f$), in which case refractive broadening will dominate. This case would apply, for example, if the fluctuations are within an order of magnitude of the scale size of the lens region itself. This was essentially the model proposed in Fiedler et al. (1987a). Clearly it is not yet possible to definitively evaluate the relative contributions of refractive and diffractive effects in the ESEs presented here. Certainly, refraction must account for the 8.1 GHz spikes in the 0954+658 event, however.

The nature of the ray-broadening process and the underlying electron density inhomogeneities can be examined using VLBI observations of sources undergoing an event. There are very definite differences among refractively and diffractively broadened images (Dennison et al. 1988; Goodman & Narayan 1985) and images which result from deterministic effects by a coherent structure as proposed by Romani (1988).

Interestingly, the statistical model agrees well with a remarkable period of anomalous disturbances of radio waves from the Crab pulsar (Lyne & Thorne 1975). The event was observed as a large increase in the pulse width. The duration of the event (about 4 months), inferred from the pulse-broadening parameters and density contrast, clearly identify it as an ESE. Moreover, the radio light curve shows a very deep rounded minimum coincident with the interval of large pulse broadening. Although Lyne & Thorne did not interpret the minimum as a direct result of diffraction or refraction, we argue that observing a minimum coincident with an independent measurement of enhanced pulse broadening is a direct confirmation of the statistical model. The broadened pulse shape is in a sense a crude one-dimensional map of the redistributed intensity. As Lyne & Thorne note, this effective intensity distribution is frequently lumpy and changes over a period of days to weeks. Clearly, these lumps indicate the presence of refractive effects.

7. CONCLUSIONS

As is illustrated in Figure 1, ESEs display a wide variety in shape, amplitude, and duration. The event shapes include paired maxima surrounding a prolonged and usually flat minimum, a rounded minimum with or without surrounding maxima, and groupings of two or more events. ESEs are found to range in duration from 0.25 to 1.2 yr and have a maximum deviation from the mean from 6% to 100% at 2.7 GHz.

A statistical model has been offered for comparison with observations and other potential models for ESEs. In this model, the variety of the ESEs may be attributable to differences in the relative angular sizes between the background extragalactic source, the lens, and the broadening angle over which the intrinsic emission is spread. Source components comparable to, but smaller than, a lens will dominate the character of the variations associated with an ESE. Furthermore, the fraction of the total source flux density in that component must be significant for the ESE variations to be distinguishable from other causes of variability in radio light curves, such as RISS or variations intrinsic to the source itself. Also, complex source or lens structures could be responsible for the repetitive time dependence of some ESEs.

Although direct observations of the material responsible for extreme scattering have yet to be obtained, the clumped spatial distribution of ESEs suggests that this material may be associated with well-known, but poorly understood, Galactic loops or spurs. ESEs are found to be clumped in the region coincident with the North Polar Spur (Loop I), and near the Galactic anticenter where the Galactic continuum Loops III and IV intersect (Fig. 4). These loops may provide the conditions that are apparently necessary for extreme scattering to occur, i.e., long path lengths in regions of enhanced turbulence in the electron density distribution.

The Green Bank interferometer is currently monitoring 150 compact extragalactic radio sources every other day. When the next occurrence of a large ESE is observed, observations will be initiated on other instruments during and after the event in the hope of studying more directly the lens itself.

We wish to thank Jim Cordes and Andrew Clegg for comments on the manuscript. We also wish to thank the NRAO staff of the Green Bank interferometer, in particular W. Cambell, F. Ghigo, L. Howell, and K. Lehman, for their diligence in maintaining this instrument and for their prompt responses to our numerous queries. We would also like to thank the USNO, without whose support the daily monitoring of large numbers of radio sources would not be possible in astronomy today. This research was supported by the Office of Naval Research.

APPENDIX A

THE STATISTICAL MODEL FOR FLUX REDISTRIBUTION

The model used to generate the light curves in Figure 3 assume a band-shaped geometry for the lens when projected on the sky (see Fig. 5*a*). The size of the long axis of the rectangular band is considered to be much larger than all other relevant angles in the problem. The angular width of the band is θ_l. Because of this geometry, no generality is lost by assuming a relative motion that carries the background source perpendicular to the long axis of the band. Other straight-line paths in relative motion will merely effect a scale change along the temporal axis of the resulting light curve. The background source is assumed to have a circular Gaussian brightness distribution with a FWHM of θ_s. Furthermore, all parallel ray bundles incident on the lens are assumed to be broadened into a Gaussian brightness distribution of FWHM θ_b (see Fig. 5*b*).

The redistributed flux density from each individual point in the two-dimensional lens is a convolution between the source brightness distribution and the broadening function. Since both of these quantities are normally distributed, the resulting distribution is also a normal function whose standard deviation is equal to the standard deviations of the source and broadening functions summed in quadrature:

$$I(\rho) = \frac{4 \ln 2}{\pi(\theta_s^2 + \theta_b^2)} e^{-4\rho^2 \ln 2/(\theta_s^2 + \theta_b^2)}, \tag{A1}$$

where the integrated source brightness has been assumed to be unity and ρ is the radial angular distance from a given point in the band. We have also assumed strong broadening; e.g., when the source is behind and much smaller than the band, all of its flux is redistributed. Note that equation (A1) is independent of the geometry of the lens. The redistributed flux density at y, the angular coordinate perpendicular to the long axis of the band, may be obtained by integrating equation (A1) over the two-dimensional area of the band:

$$F_{\rm scat}(d) = \int_{d-\theta_l/2}^{d+\theta_l/2} \int_{-\infty}^{+\infty} I(\rho = \sqrt{x^2 + y^2}) dx\, dy, \tag{A2}$$

where x is the angular coordinate parallel to the long axis of the band and d is the y-coordinate of the background source (see Fig. 5*a*). The origin of the y-axis is at the center of the band. Similarly, the direct flux density is

$$F_{\rm unscat}(d) = \int_{\theta_l/2-d}^{+\infty} \int_{-\infty}^{+\infty} B(\rho) dx\, dy + \int_{-\infty}^{-\theta_l/2-d} \int_{-\infty}^{+\infty} B(\rho) dx\, dy, \tag{A3}$$

where $B(\rho)$ is the assumed source brightness distribution,

$$B(\rho) = \frac{4 \ln 2}{\pi \theta_s^2} e^{-4\rho^2 \ln 2/\theta_s^2}. \tag{A4}$$

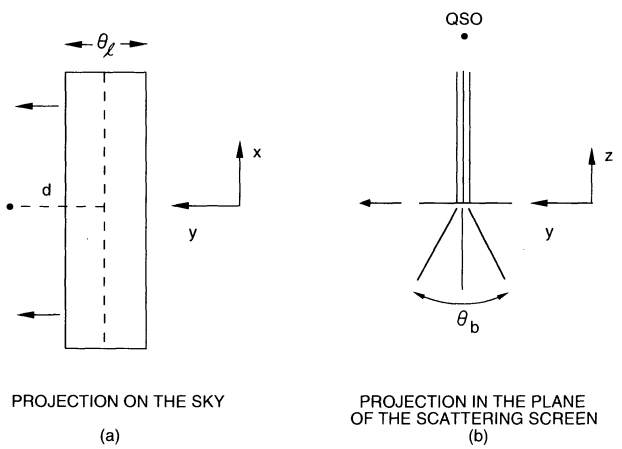

FIG. 5.—Band-shaped geometry of the lens region shown (*a*) from the perspective of the observer and (*b*) from the plane of the lens

Combining equations (A2) and (A3) and performing the substitutions indicated in equations (A1) and (A4) gives the normalized form of the light curve for a band-shaped lens

$$F(d) = N[c(d - \theta_l/2)/\sigma_{\rm scat},\ c(d + \theta_l/2)/\sigma_{\rm scat}] + N[c(\theta_l/2 - d),\ +\infty] + N[-\infty,\ c(-\theta_l/2 - d)]\ , \tag{A5}$$

where θ_s is assumed to be unity, $c^2 = 8 \ln 2$, $\sigma^2_{\rm scat} = 1 + \theta_b^2$, and

$$N[a, b] = \frac{1}{\sqrt{2\pi}} \int_a^b e^{-v^2/2}\, dv\ . \tag{A6}$$

In deriving equation (A5) we have assumed that the FWHM θ_b of the broadening function is constant across the lens. Generalizing the problem to include arbitrary geometries for the bounds of the lens and an arbitrary dependence of θ_b on position across the lens is straightforward. However, until a detailed understanding of the milliarcsecond structure of the background sources is obtained, one must be careful not to over interpret the observational data with respect to this, or any other, model attempting to describe extreme scattering events.

APPENDIX B

MEAN AND VARIANCE OF W

As described in the text, the test statistic W used to evaluate the relative "nearness" of event sources to loops was the sum of ranks R_i of the m event sources, where all N sources are ranked in order of distance from the nearest loop. Under the null hypothesis that the locations of the event sources are unrelated to the loops, and therefore that their ranks are completely random, the expectations of W and W^2 are readily calculated as

$$\langle W \rangle = \sum_{i=1}^{m} \langle r_i \rangle = \frac{m(N+1)}{2} \tag{B1}$$

and

$$\langle W^2 \rangle = \sum_{i=1}^{m} \langle r_i^2 \rangle + 2 \sum_{i=1}^{m-1} \sum_{j=i+1}^{m} \langle r_i r_j \rangle$$
$$= \frac{m(N+1)(2N+1)}{6} + \frac{m(m-1)}{N(N-1)} \left\{ N^2 \left(\frac{N+1}{2} \right)^2 - N \left[\frac{(N+1)(2N+1)}{6} \right] \right\}. \tag{B2}$$

The variance of W is then found to be

$$\sigma_W^2 \equiv \langle W^2 \rangle - \langle W \rangle^2 = \frac{m(N-m)(N+1)}{12}\ . \tag{B3}$$

For sufficiently large N, the distribution of W approaches a Gaussian with mean $\langle W \rangle$ and standard deviation σ_W. Rather than attempt to calculate the sample size required for the Gaussian approximation to be valid, we check the inferred frequency of occurrence of a set of outcomes (i.e., $W \leq W_m$, where W_m is a measured value) by Monte Carlo simulation as described in the text.

REFERENCES

Altschuler, D. R., Broderick, J. J., Condon, J. J., Dennison, B., Mitchell, K. J., O'Dell, S. L., & Payne, H. E. 1984, AJ, 89, 1784
Antonucci, R. R. J., & Ulvestad, J. S. 1985, ApJ, 294, 158
Armstrong, J. W., Coles, W. A., Kojima, M., & Rickett, B. J. 1990, ApJ, 358, 685
Berkhuijsen, E. M., Haslam, C. G. T., & Salter, C. J. 1971, A&A, 14, 252
Blandford, R., & Narayan, R. 1985, MNRAS, 213, 591
Clegg, A. W., Chernoff, D., & Cordes, J. M. 1988, in Radio Wave Scattering in the Interstellar Medium, ed. J. Cordes, B. Rickett, & D. Backer (New York: AIP), 174
Cordes, J. M., Pidwerbetsky, A., & Lovelace, R. V. E. 1986, ApJ, 310, 737
Cordes, J. M., Weisberg, J. M., & Boriakoff, V. 1985, ApJ, 288, 221
Dennison, B., Broderick, J. J., O'Dell, S. L., Mitchell, K. J., Altschuler, D. R., Payne, H. E., & Condon, J. J. 1984a, ApJ, 281, 55
Dennison, B., Fiedler, R. L., & Johnston, K. J. 1988, in IAU Symp. 129, The Impact of VLBI on Astrophysics and Geophysics, ed. M. J. Reid & J. M. Moran (Dordrecht: Kluwer), 299
Dennison, B., Thomas, M., Booth, R. S., Brown, R. L., Broderick, J. J., & Condon, J. 1984b, A&A, 135, 199
Diamond, P. J., Goss, W. M., Romney, J. D., Booth, R. S., Kalberla, P. M. W., & Mebold, U. 1989, ApJ, 347, 302
Dieter, N. H., Welch, W. J., & Romney, J. D. 1976, ApJ, 208, 113
Fey, A. L., Clegg, A. W., & Fiedler, R. L. 1994, in preparation
Fiedler, R. L., Dennison, B., Johnston, K. J., & Hewish, A. 1987a, Nature, 326, 675
Fiedler, R. L., Dennison, B., Simon, R., & Johnston, K. J. J. 1993a, in preparation
Fiedler, R. L., Pauls, T., Johnston, K. J. J., & Dennison, B. 1993b, ApJ, submitted
Fiedler, R., et al. 1987b, ApJS, 65, 319
Goodman, J., & Narayan, R. 1985, MNRAS, 214, 519
Heeschen, D. S. 1984, AJ, 89, 1111
Higdon, J. C. 1984, ApJ, 285, 109
Kellermann, K. I., & Pauliny-Toth, I. I. K. 1981, ARA&A, 19, 373
Lawrence, C. R., et al. 1985, ApJ, 296, 458
Lyne, A. G., & Thorne, D. J. 1975, MNRAS, 172, 97
Marscher, A. P. 1988, ApJ, 334, 552
Marscher, A. P., Broderick, J. J., Padrielli, L., Bartel, N., & Romney, J. D. 1987, ApJ, 319, 456
Marscher, A. P., & Shaffer, D. B. 1980, AJ, 85, 668
Narayan, R., Anantharamaiah, K. R., & Cornwell, T. J. 1989, MNRAS, 241, 403
Pearson, T. J., & Readhead, A. C. S. 1981, ApJ, 248, 61
———. 1988, ApJ, 328, 114
Preston, R. A., Morabito, D. D., Williams, J. G., Faulkner, J., Jauncy, D. L., & Nicholson, G. D. 1985, AJ, 90, 1599
Rickett, B. J. 1986, ApJ, 307, 564
———. 1990, ARA&A, 28, 561
Romani, R. W. 1988, in Radio Wave Scattering in the Interstellar Medium, ed. J. Cordes, B. Rickett, & D. Backer (AIP Conf. Ser. 174), 156
Romani, R. W., Blandford, R. D., & Cordes, J. M. 1987, Nature, 328, 324
Romney, J., et al. 1984, A&A, 135, 289
Shapirovskaya, N. Ya. 1978, Soviet Astron.—AJ, 22, 544
Simonetti, J. H., Cordes, J. M., & Heeschen, D. S. 1985, ApJ, 296, 46
Waltman, E. B., Fiedler, R., Johnston, K. J., Spencer, J. H., Florkowski, D. R., Josties, F. J., McCarthy, D. D., & Matsakis, D. N. 1991, ApJS, 77, 379
Weiler, K. W., & Johnston, K. J. 1980, MNRAS, 190, 269
Zensus, J. A., Procas, R. W., & Pauliny-Toth, I. I. K. 1984, A&A, 133, 27